Supporting Information

Enhanced Full-Seawater Splitting with CoNiP@N, P-C Core-Shell Electrocatalyst

Fangyou Meng, Qing Chen, Kaiyi Shi*, Shuangzhu Jia, Xuexin Dai*

School of Chemistry and Chemical Engineering, Qiannan Normal University for Nationalities, Duyun, 558000, China.

Corresponding authors: Kaiyi Shi (K. Y. Shi), Xuexin Dai (X. X. Dai)

Email: andrewshikai@sgmtu.edu.cn; daixuexin@sgmtu.edu.cn

Experimental section

Electrochemical measurement

The electrocatalytic properties of the as-synthesized samples were measured by an electrochemical analysis station (PGSTAT302N, Metrohm, Switzerland) in a typical three-electrode system at 298 K. The as-prepared CoNiP@N,P-C, Hg/HgO and graphite were applied to the working electrode, reference electrode and counter electrode, respectively. Typically, 5 mg of as-synthesized CoNiP@N,P-C nanoparticle electrocatalyst was dissolved 950 μl of ethanol and 50 μl of Nafion by ultrasound for 30 min. 20 μl of ink was dropped onto the carbon cloth (1 cm x 1 cm) and dried at room temperament. 1 M KOH electrolyte was purged by N_2(99.999%) for 30 min to dislodge the redundant oxygen

before each test. All electrocatalytic performances were assessed by linear sweep voltammetry (LSV) curve at 2 mV/s scan rate. All the potentials were calculated by the formula (E_{RHE} = $E_{(Hg/HgO)}$ + 0.098+ 0.059 x pH). The double-layer capacitance (C_{dl}) of the electrocatalyst was assessed by testing CV at a scan rate (10-200 mV/s). Electrochemical impedance spectroscopy was measured by amplitude of 5 mV at frequency range of 1 Hz-10^5 Hz. For comparison, the commercial 20% Pt/C, NiP@N, P-C and CoP@N, P-C were prepared into ink and it was loaded onto the pure carbon clothe with the same load.

Density Functional Theory Calculation Details

The first-principles were employed to perform all density functional theory (DFT) calculations within the generalized gradient approximation (GGA) using the Perdew-Burke-Ernzerhof (PBE)formulation. The projected augmented wave (PAW) potentials were used for describing the ionic cores and take valence electrons into account using a plane wave basis set with a kinetic energy cutoff of 520 eV. Partial occupancies of the Kohn−Sham orbitals were allowed using the Gaussian smearing method with a width of 0.05 eV. The electronic energy was considered self-consistent when the energy change was smaller than 10^{-5} eV. A geometry optimization was considered convergent when the energy change was smaller than 0.05 eV Å−1. In our structure, the U correction is used for Co atoms with 4.29 eV for d states. The vacuum spacing in a

direction perpendicular to the plane of the structure is 20 Å for the surfaces. The Brillouin zone integration is performed using 2×2×1 Monkhorst-Pack k-point sampling for a structure. Finally, the adsorption energies(Eads) were calculated as Eads= Ead/sub -Ead -Esub, where Ead/sub, Ead, and Esub are the total energies of the optimized adsorbate/substrate system, the adsorbate in the structure, and the clean substrate, respectively. The free energy was calculated using the equation:

G=Eads+ZPE-TS

where G, Eads, ZPE and TS are the free energy, total energy from DFT calculations, zero point energy and entropic contributions, respectively.

Results and Discussions

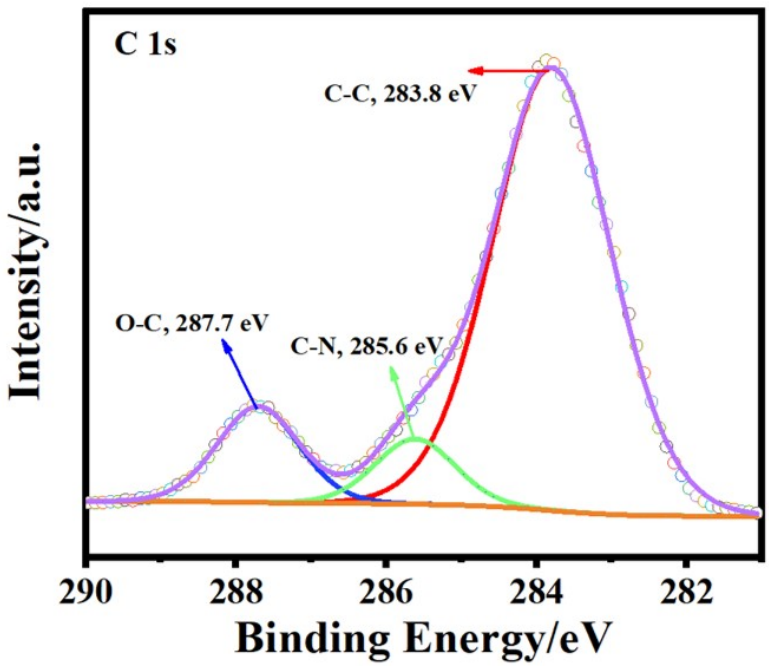

Figure S1. XPS spectra of C 1s of the CoNiP@N,P-C.

The the chemical bonds of the CoNiP@N,P-C hybrids catalysts were characterized by XPS, and the results were shown in Figure S1. The high-resolution C 1s spectrum in Figure S1 (Supporting Information) can be fitted into three peaks of C-C (283.8 eV, sp^2-hydridized carbon), C-N (285.6 eV), and C-O (287.7 eV).

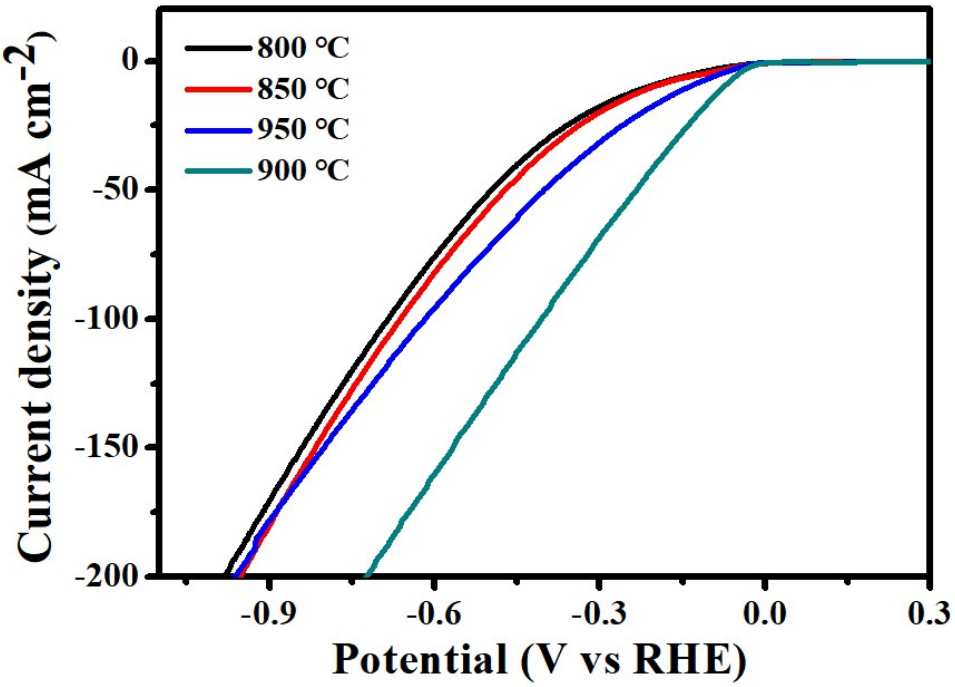

Figure S2. Electrochemical performance of the CoNiP@N, P-C catalyst, LSV curves of CoNiP@N, P-C catalyst catalyst HER at different temperatures in 1 M KOH alkaline solution.

Temperature is one of the factors affecting the catalytic activity of the catalyst. As shown in Figure S2, the effects of different temperatures on the catalytic performance of the CoNiP@N, P-C catalyst were investigated. The overpotential of the catalyst at 900 ℃ carbonization temperature was the lowest (76 mV) compared to 800 ℃ (213 mV), 850 ℃ (202 mV), 950 ℃ (137 mV), reaching a current density of 10 mA

cm^{-2}. The crystallinity of the material may improve with the increase of temperature, but the relative content of N and P and the surface area of the sample decrease, which leads to the decrease of catalytic performance. Therefore, the reaction temperature of the system was 900 ℃ to prepare CoNiP@N, P-C catalyst.

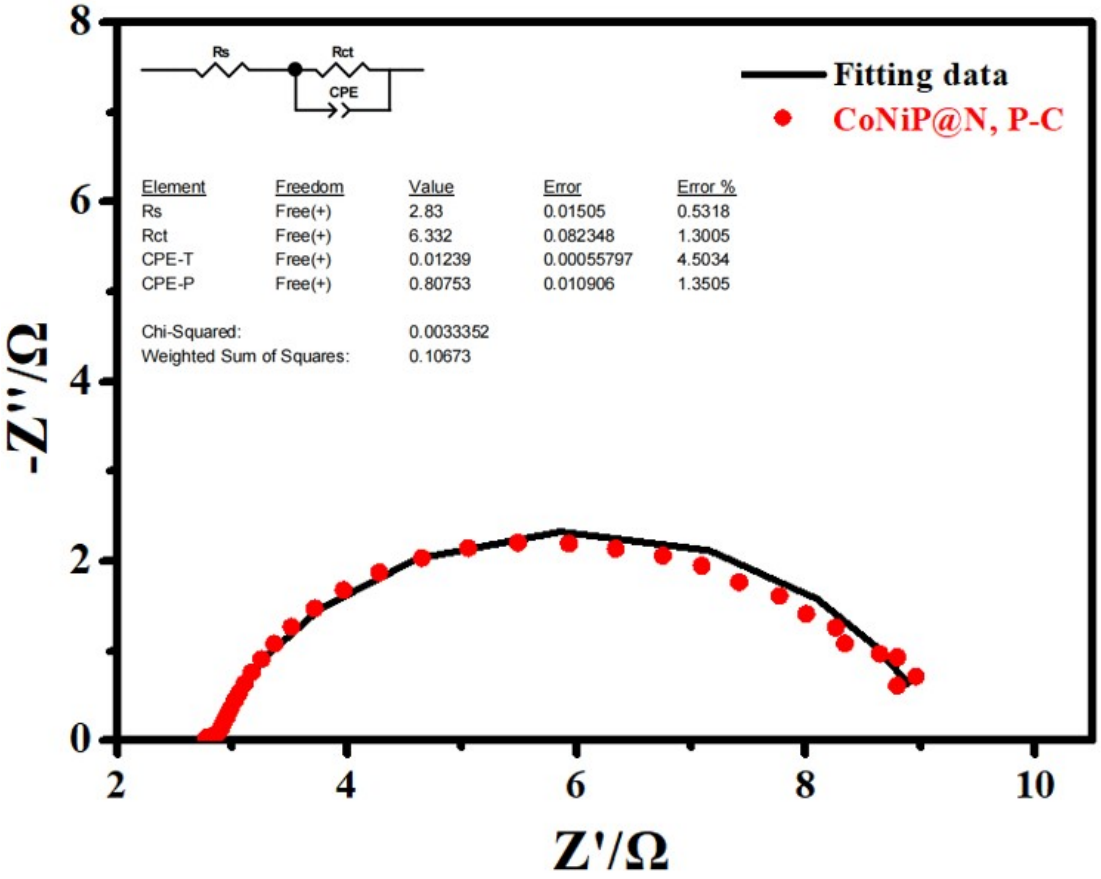

Figure S3. The Fitting results of EIS test date of CoNiP@N, P-C.

Electrochemical impedance spectroscopy (EIS) experiments were used to examine the charge transfer kinetics of the samples. Figure S3 shows the fitting Nyquist plots of the CoNiP@N, P-C catalyst. The fitting results indicate that the CoNiP@N, P-C electrode shows a notably lower charge transfer resistance (6.3 Ω).

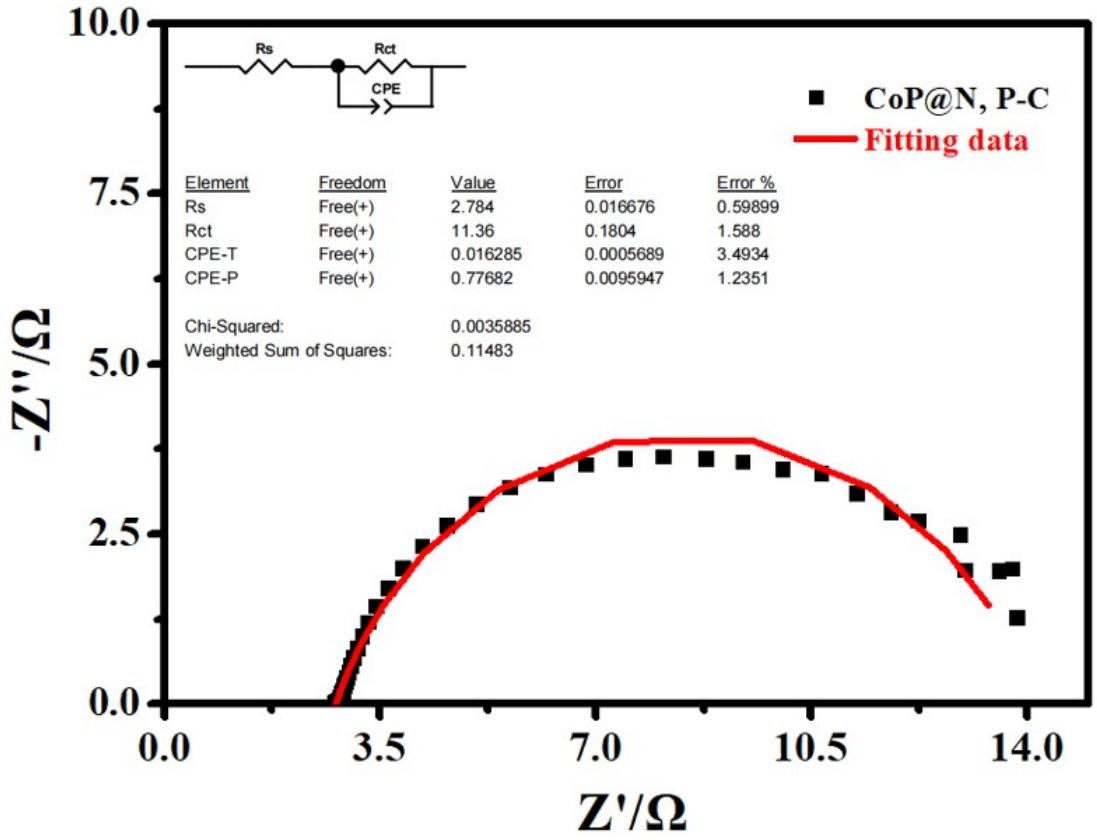

Figure S4. The Fitting results of EIS test date of CoP@N, P-C.

The Figure S4 shows the fitting Nyquist plots of the CoP@N, P-C catalyst. The fitting results indicate that the CoP@N, P-C electrode shows a notably lower charge transfer resistance (11.3 Ω).

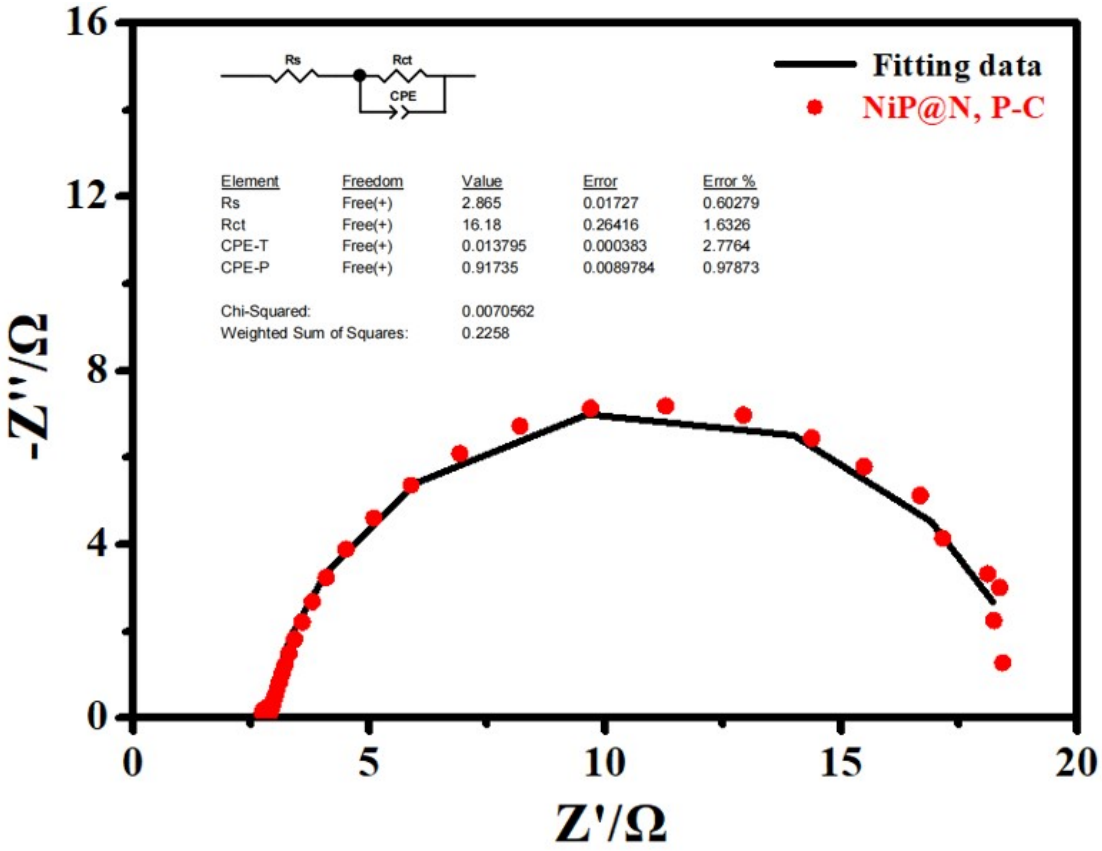

Figure S5. The Fitting results of EIS test date of NiP@N, P-C.

The Figure S5 shows the fitting Nyquist plots of the NiP@N, P-C catalyst. The fitting results indicate that the NiP@N, P-C electrode shows a notably lower charge transfer resistance (16.1 Ω).

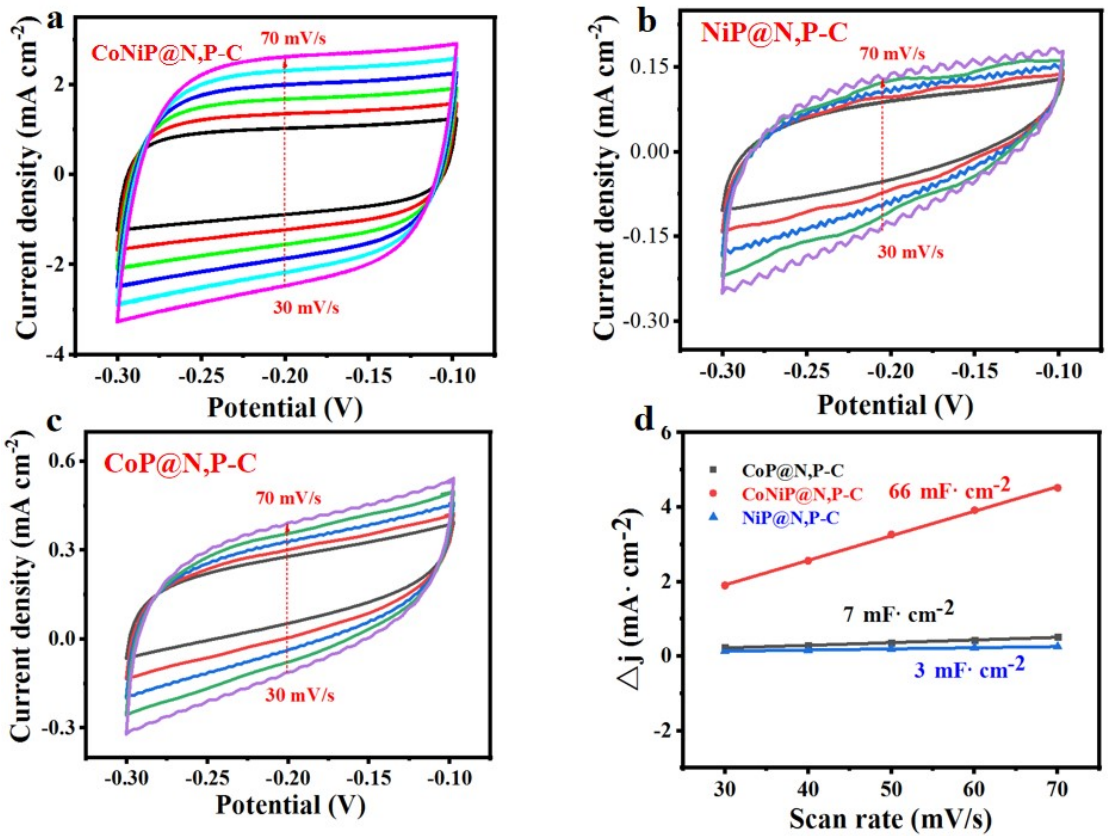

Figure S6. Electrochemical performance of catalyst, (a) Current density of CoNiP@N,P-C hybrids catalysts at different scan, (b) Current density of NiP@N,P-C at different scan, (c) Double-layer capacitance of CoP@N,P-C, CoNiP@N,P-C hybrids catalysts calculated according to the CV curves.

To estimate the as-prepared sample intrinsic electrocatalytic activity, the double-layer capacitance (C_{dl}) of the CoNiP@N,P-C hybrids catalysts was measured to inspect electrochemically active surface area. According to the previous reports, at the same potential window, to evaluate the C_{dl}, the different CVs of the three different work electrodes were measured under the scan rate ranging from 30 to 70 mV s^{-1}, and the results were shown in Figure S6.

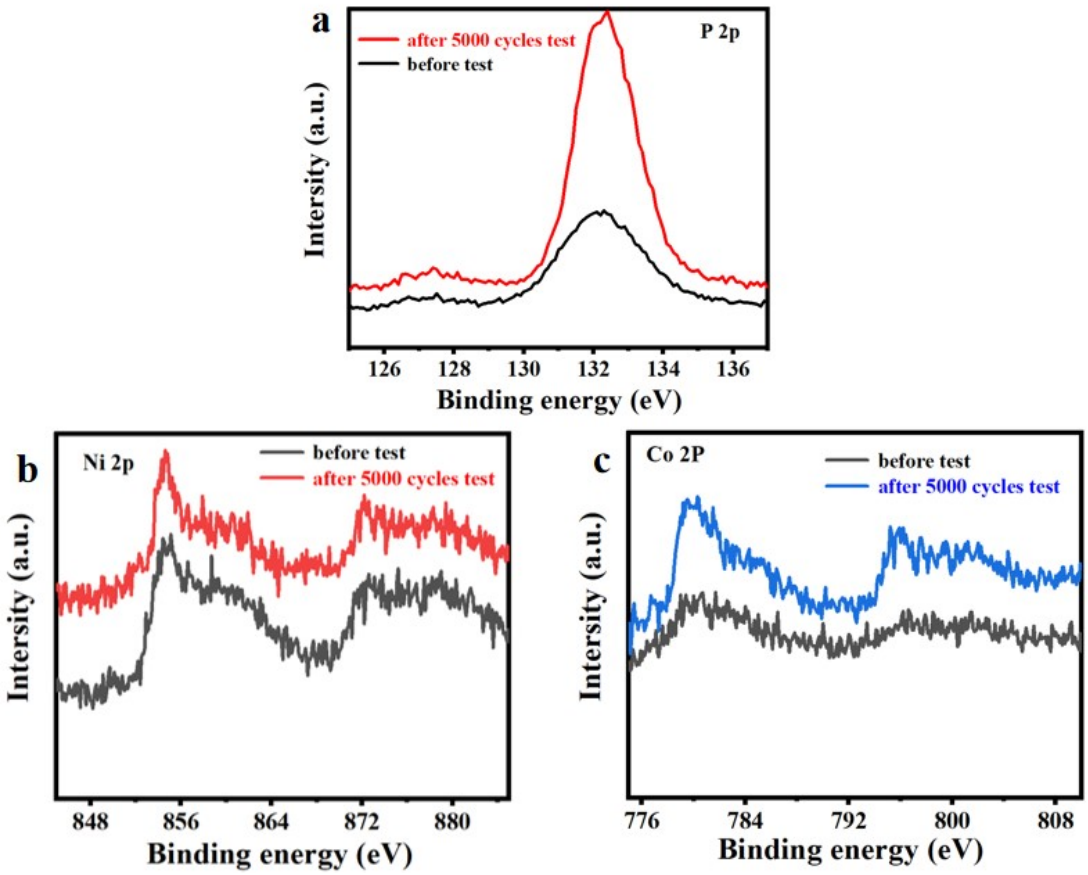

Figure S7. (a) XPS spectra of (a) P 2p, (b) Ni 2p , (c) Co 2p of the CoNiP@N,P-C hybrids catalysts before test and after 5000 cycles test

The X-ray photoelectron spectroscopy (XPS) experiments of the sample after 5000 cycles was carried out, and the results were shown in Figure S7. The valence state of Co 2p, Ni 2p and P 2p had no significant change, further suggesting that the CoNiP@N,P-C hybrids catalysts electrode had good stability.

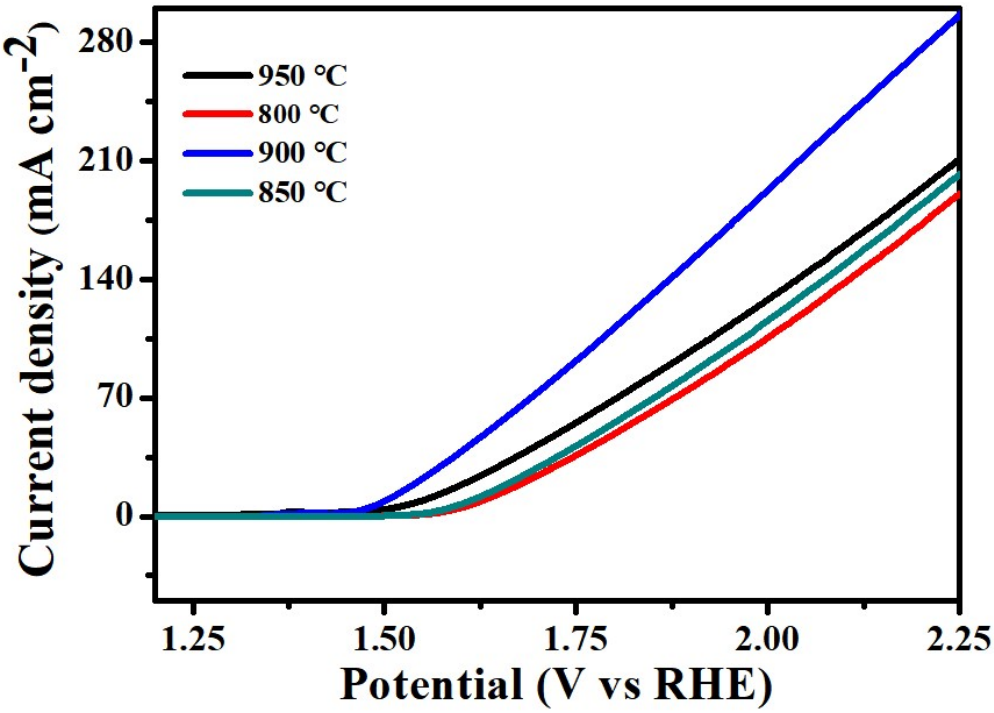

Figure S8. Electrochemical performance of the CoNiP@N, P-C catalyst, LSV curves of CoNiP@N, P-C catalyst catalyst OER at different temperatures in 1 M KOH alkaline solution.

As shown in Figure S8, the overpotential of the catalyst at 900 ℃ the reaction temperature was the lowest (270 mV) compared to 800 ℃ (402 mV), 850 ℃ (387 mV), 950 ℃ (324 mV), reaching a current density of 10 $mV \cdot cm^{-2}$. Therefore, the reaction temperature of the system was 900 ℃ to prepare CoNiP@N, P-C catalyst.

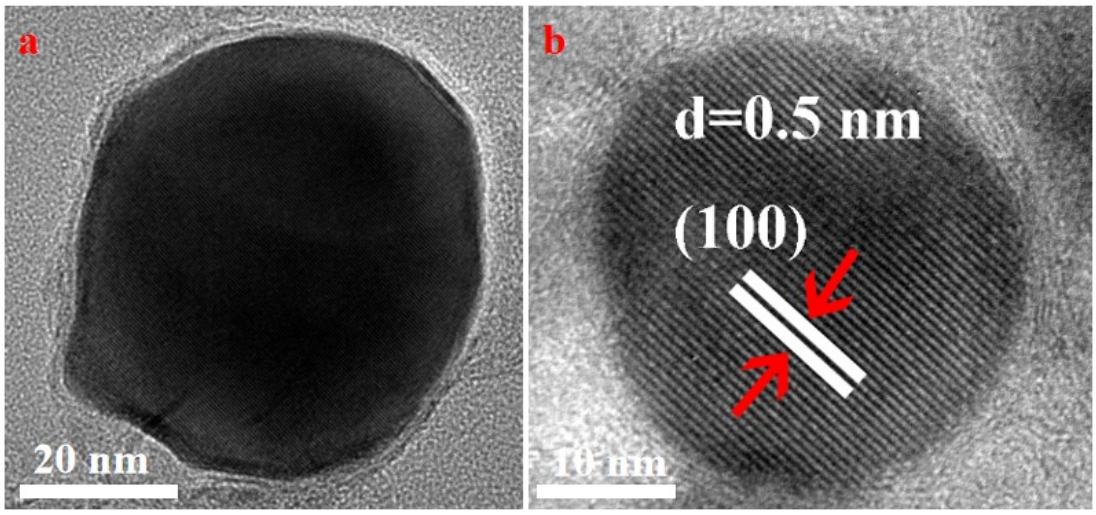

Figure S9 (a) TEM images of CoNiP@N,P-C hybrids catalysts before testing for HER, (b) TEM images of CoNiP@N,P-C hybrids catalysts after the 5000 cycles for HER.

The stability of the catalyst after 5000 cycles was evaluated by observing the changes of the samples before and after the test via transmission microscope (TEM), and the results are shown in Figure S9a and 9b, taken from the sample before testing and after the 5000 cycles, respectively, showing that the crystal structure of nanoparticles did not change after long cycle test. The 0.5 nm interplanar crystal spacing shown in the 5000 cycles testing sample, correspond to the (100) crystal plan of CoNiP (JCPDS 71-2336), which was consistent with the structure of the sample before testing. These results shown that the CoNiP@N,P-C hybrids catalysts electrode had good stability, and the appearance and structure remained relatively stable after the 5000 cycles.

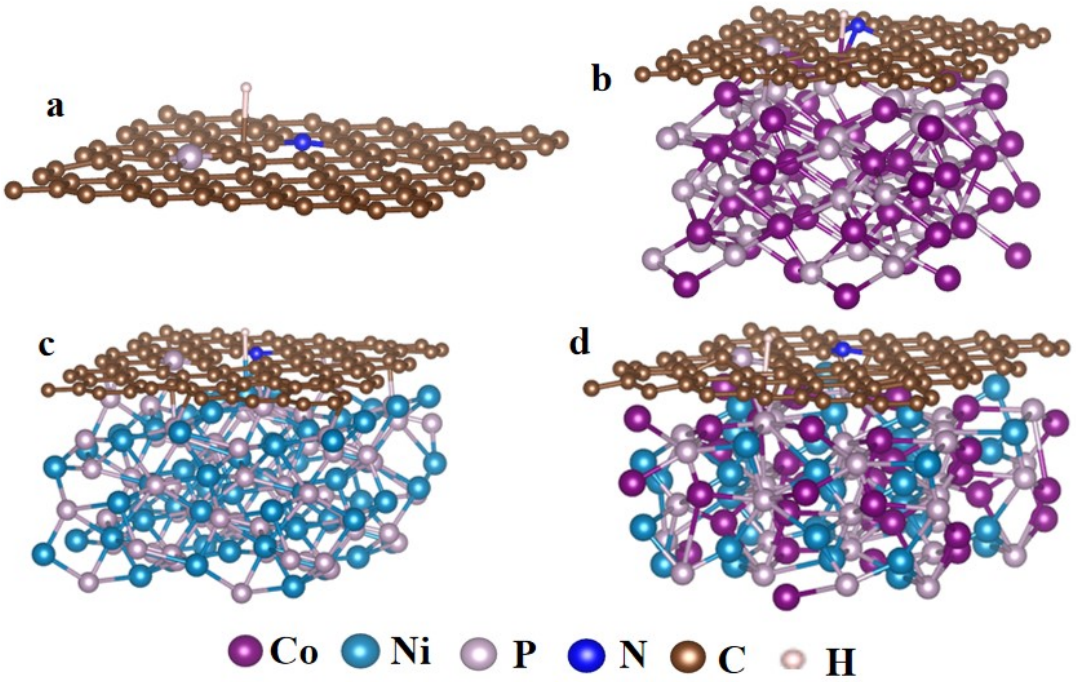

Figure S10. (a) Stable model of hydrogen in N, P-C, (b) Stable model of hydrogen in CoP@N, P-C, (c) Stable model of hydrogen in NiP@N, P-C, (d) Model of hydrogen in CoNiP@N, P-C (purple represent cobalt, blue represent nitrogen, pink represent phosphorus, blue represent nitrogen, baby blue represent hydrogen, gold represent carbon, light gold represent hydrogen).

To illuminate of the intrinsic connecting link between the elect-ronic structure and the high catalytic activity toward HER of asprepared CoNiP@N,P-C catalyst, the first principle calculations were carried out using density functional theory. Figure S10a, S10b, S10c and S10d represented hydrogen in N,P-C, CoP@N,P-C, NiP@N,P-C and CoNiP@N,P-C structural models, respectively. Stable models (red represent cobalt, blue represent nitrogen, pink represent phosphorus, blue represent nitrogen, gold represent carbon, light gold represent hydrogen)

of CoNiP@N,P-C.

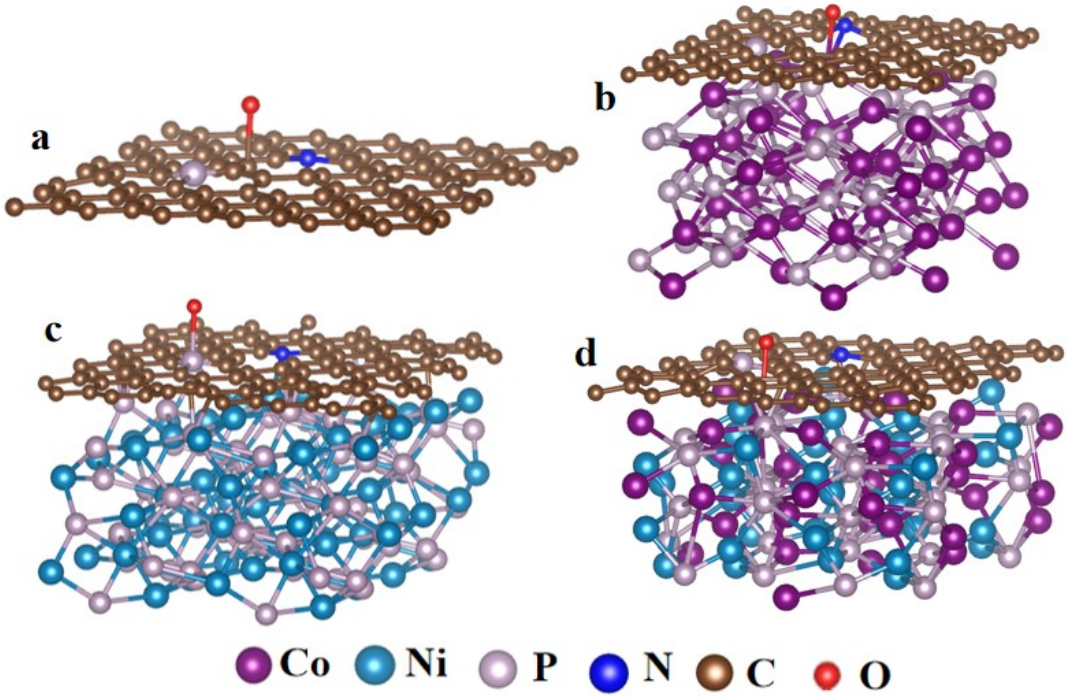

Figure S11 (a) Stable model of oxygen in N,P-C, (b) Stable model of oxygen in CoP@N,P-C, (c) Stable model of oxygen in NiP@N,P-C, (d) Model of oxygen in CoNiP@N,P-C (purple represent cobalt, blue represent nitrogen, pink represent phosphorus, blue represent nitrogen, gold represent carbon, red represent oxygen).

To illuminate of the intrinsic connecting link between the elect-ronic structure and the high catalytic activity toward OER of asprepared CoNiP@N,P-C catalyst, the first principle calculations were carried out using density functional theory. Figure S11a, S12b, S13c and S14d represented hydrogen in N,P-C, CoP@N,P-C, NiP@N,P-C and CoNiP@N,P-C structural models, respectively. Stable models (purple represent cobalt, blue represent nitrogen, pink represent phosphorus, blue represent nitrogen, gold represent carbon, red represent oxygen) of

CoNiP@N,P-C.

Table S1. Comparison HER performance of different catalysts in 1M KOH

Catalyst	Elecolyte	η at j=10 mA cm^{-2}	Reference
Zn-Co-P	1M KOH	172 mV	1
MoP-RGO	1M KOH	150 mV	2
Mn-FeP	1M KOH	173 mV	3
FeP/NCNSs	1M KOH	409 mV	4
NiFeS	1M KOH	315 mV	5
Co-C-NF	1M KOH	178 mV	6
NiCoFe LTHs	1M KOH	200 mV	7
Co_9S_8-NixSy	1M KOH	163 mV	8
CoNiP@N,P-C	**1M KOH**	**76 mV**	**This work**

Table S2. Comparison OER performance of different catalysts in 1M KOH

Catalyst	Elecolyte	η at j=10 mA cm^{-2}	Reference
Mo－N/C@MoS_2	1M KOH	390 mV	9
Co@N-CNTF	1M KOH	350 mV	10
SCF0.15	1M KOH	380 mV	11
Co_3O_4/HNCP	1M KOH	333 mV	12
NiCoS/Ti_3C_2Tx	1M KOH	365 mV	13
$Co_{0.13}Ni_{0.87}Se_2$	1M KOH	320 mV	14
Co89%Ni11%Ox(OH)y	1M KOH	450 mV	15
$NiCo_2O_4$ nanowires	1M KOH	450 mV	16
CoNiP@N,P-C	**1M KOH**	**270 mV**	**This work**

Table S3. Comparison full water splitting performance of different catalysts in 1M KOH

catalyst	HER (mV) at 10 mV cm^{-2}	OER (mV) at 10 mV cm^{-2}	Overall water splitting (V) at 10 mV cm^{-2}	Reference
Ni/Mo_2C-PC	179	368	1.66	17
Co-NC@ Mo_2C	99	347	1.685	18
CoP/rGO	150	340	1.71	19
Co_9S_8@MoS_2	143	342	1.67	20
$Co_{0.85}$Se@NC	230	320	1.76	21
NiS_2/CoS_2-O	174	235	1.768	22
NiFeLDH/NF	210	240	1.7	23
CoP/PNC	165	300	1.68	24
$Co(OH)_2$@NC NTs@ NF	170	270	1.72	25
CoNiP@N,P-C	**76**	**270**	**1.54**	**This work**

References

1.Y.Q. Jing, H.L. Liu, R.J. Yan, J. Chen, H.T. Dai, C.L. Liu, Mesoporous CoP Nanowire Arrays for Hydrogen Evolution, ACS Appl. Nano Mater. 2(2019) 5922−5930.

2. Z.X. Wu, J. Wang, J. Zhu, J.P. Gao, W.P. Xiao, C.J. Xuan, W. Le, D.L. Wang, Highly efficient and stable MoP-RGO nanoparticles as electrocatalysts for hydrogen evolution, Electrochimica Acta, 232(2017) 254-261.

3. M. Wang, Y.X. Tuo, X.K. Li, Q.F. Hua, F.L. Du, L. H. Jiang, Mesoporous Mn-Doped FeP: Facile Synthesis and Enhanced Electrocatalytic Activity for Hydrogen Evolution in a Wide pH Range, ACS Sustainable Chem. Eng. 7(2019)

12419−12427.

4. Y. Yang, P. Zhuo, A. Muhammad, H.T. Wang, W. Wang, Z.X. Wu, Z.Y. Wang, X.Y. Qiu, H. Tan, FeP Nanocrystals Embedded in N-Doped Carbon Nanosheets for Efficient Electrocatalytic Hydrogen Generation over a Broad pH Range, ACS Sustainable Chem. Eng. (2018) 8b01746-.
5. P. Ganesan, A. Sivanantham, S. Shanmugam. Inexpensive Electrochemical Synthesis of Nickel Iron Sulfides on Nickel Foam: Super Active and Ultra-durable Electrocatalysts for Alkaline Electrolyte Membrane Water Electrolysis. J. mater. chem. A, (2016) 10.1039.C6TA04499A.
6. Z. L. Wang, X. F. Hao, Z. Jiang, X. P. Sun, D. Xu, J. Wang, H. X. Zhong, F. L. Meng, X. B. Zhang. C and N Hybrid Coordination Derived Co–C–N Complex as a Highly Efficient Electrocatalyst for Hydrogen Evolution Reaction. J. Am. Chem. Soc. 137 (2015) 15070−15073.
7. A.-L. Wang, H. Xu, G.-R. Li. NiCoFe Layered Triple Hydroxides with Porous Structuresas High-Performance Electrocatalysts for Overall Water Splitting. ACS Energy Lett. 1 (2016) 445−453.
8. D. Ansovini, C. J. J. Lee, C. S. Chua, L. T. Ong, H. R. Tan, W. R. Webb, R. Raja, Y.-F. Lim. Highly active hydrogen evolution electrocatalyst based on cobalt-nickel sulfide composite electrode. J. Mater. Chem. A. 4 (2016) 9744-9749.
9. I. S. Amiinu, Z. Pu, X. Liu, K. A. Owusu, H. G. R. Monestel, F. O. Boakye, H. Zhang, S. Mu. Multifunctional Mo-N/C@MoS_2 Electrocatalysts for HER, OER, ORR, and Zn-Air Batteries. Adv. Funct. Mater. 27(2017) No.1702300.
10. H. Guo, Q. Feng, J. Zhu, J. Xu, Q. Li, S. Liu, K. Xu, C. Zhang, T. Liu. Cobalt nanoparticle-embedded nitrogen-doped carbon/carbon nanotube frameworks derived from a metal–organic framework for tri-functional ORR, OER and HER electrocatalysis. J. Mater. Chem. A. 7 (2019), 3664-3672.
11. W. Wang, Y. Yang, D. Huan, L. Wang, N. Shi, Y. Xie, C. Xia, R. Peng, Y. Lu. An excellent OER electrocatalyst of cubic $SrCoO_3$−δ prepared by a simple Fdoping strategy. J. Mater. Chem. A. 7 (2019), 12538-12546.

12. D. Ding, K. Shen, X. Chen, H. Chen, J. Chen, T. Fan, R. Wu, Y. Li. MultiLevel Architecture Optimization of MOF-Templated Co-Based Nanoparticles Embedded in Hollow N-Doped Carbon Polyhedra for Efficient OER and ORR. ACS Catalysis. 8 (2018), 7879-7888.
13. H. Y. Zou, B. W. He, P. Y. Kuang, J. G. Yu, K. Fan. Metal-Organic Framework-Derived Nickel-Cobalt Sulfide on Ultrathin Mxene Nanosheets for Electrocatalytic Oxygen Evolution. ACS Appl. Mater. Interfaces. 10(2018) 22311−22319
14. T. Liu. A. M. Asiri, X. Sun. Electrodeposited Co-doped $NiSe_2$ Nanoparticles Film: a Good Electrocatalyst for Efficient Water Splitting. Nanoscale. 8(2016) 3911-3915.
15. N. Weidler, J. Schuch, F. Knaus, Stenner, Stenner, S. Hoch, A. Maljusch, R. Schaefer, B. Kaiser, W. Jaegermann. X-ray Photoelectron Spectroscopic Investigation of Plasma Enhanced Chemical Vapor Deposited NiOx , NiOx(OH)(y), and CoNiOx ,(OH)(y): Influence of the Chemical Composition on the Catalytic Activity for the Oxygen Evolution Reaction. J. Phys. Chem. C. 121(2017) 6455-6463.
16. X. Yu, Z. Sun, Z. Yan, B. Xiang, X. Liu, P. Du. Direct Growth of Porous Crystalline $NiCo_2O_4$ Nanowire Arrays on a Conductive Electrode for H igh-Performance Electrocatalytic Water Oxidation. J. Mater. Chem. A. 2(2014) 20823-20831.
17. Z. Y. Yu, Y. Duan, M. R. Gao, C. C. Lang, Y. R. Zheng, S.H. Yu. A onedimensional porous carbon-supported Ni/Mo_2C dual catalyst for efficient water splitting. Chemical Science. 8 (2017), 968-973.
18. Q. Liang, H. Jin, Z. Wang, Y. Xiong, S. Yuan, X. Zeng, D. He, S. Mu. Metalorganic frameworks derived reverse-encapsulation Co-NC@Mo_2C complex for efficient overall water splitting. Nano Energy. 57(2019) 746-752.
19. L. Jiao, Y. X. Zhou, H. L. Jiang. Metal-Organic Framework-Based CoP/Reduced Graphene Oxide: High-Performance Bifunctional Electrocatalyst for Overall Water Splitting. Chem. Sci. 7(2016) 1690-1695.

20. J. Bai, T. Meng, D. Guo, S. Wang, B. Mao, M. Cao. Co_9S_8@MoS_2 Core-Shell Heterostructures as Trifunctional Electrocatalysts for Overall Water Splitting and Zn-Air Batteries. ACS Appl. Mater. Inter. 10(2018) 1678-1689.
21. T. Meng, J. W. Qin, S. G. Wang, D. Zhao, B. G. Mao, M. H. Cao. In Situ Coupling of $Co_{0.85}Se$ and N–Doped Carbon via One–Step Selenizing of Metal–Organic Frameworks as Trifunctional Catalysts for Overall Water Splitting and Zn–air Batteries. J. Mater. Chem. A. 5(2017) 7001-7014.
22. J. Yin, Y. Li, F. Lv, M. Lu, K. Sun, W. Wang, L. Wang, F. Cheng, Y. Li, P. Xi, S. Guo. Oxygen Vacancies Dominated NiS_2/CoS_2 Interface Porous Nanowires for Portable Zn-Air Batteries Driven Water Splitting Devices. Adv. Mater. 29(2017) 1704681.
23. J. S. Luo, J. H. Im, M. T. Mayer, M. Schreier, M. K. Nazeeruddin, N. G. Park, S. D. Tilley, H. J. Fan, M Grätzel. Water Photolysis at 12.3% Efficiency via Perovskite Photovoltaics and Earth-Abundant Catalysts. Science. 345(2014) 6204.
24. Z. Peng, Y. Yu, D. Jiang, Y. L. Wu, B. Y. Xia. Z. H. Dong. N-doped carbon shell coated CoP nanocrystals encapsulated in porous N-doped carbon substrate as efficient electrocatalyst of water splitting. Carbon. 2019.
25. P. Guo, J. Wu, X. B. Li, J. Luo, W. M. Lau, H. Liu, X. L. Sun, L. M. Liu, A highly stable bifunctional catalyst based on 3D $Co(OH)_2$@NCNTs@NF towards overall water-splitting. Nano Energy, 96(2018)-104.